Carbon budget for 1.5 and 2oC targets lowered by natural wetland and permafrost feedbacks

Article

Accepted Version

Carbon budget for 1.5 and 2ºC targets lowered by natural wetland and permafrost feedbacks

Edward Comyn-Platt[1,*], Garry Hayman[1], Chris Huntingford[1], Sarah Chadburn[2,3], Eleanor Burke[4], Anna Harper[3], William Collins[5], Christopher Webber[5], Tom Powell[4], Peter Cox[4], Nic Gedney[6], Stephen Sitch[4]

1: Centre for Ecology and Hydrology, Wallingford, OX10 8BB, U.K.

2: University of Leeds, Leeds, LS2 9JT, U.K.

3: University of Exeter, Exeter, EX4 4QF, U.K.

4: Met Office Hadley Centre, FitzRoy Road, Exeter, EX1 3PB, U.K.

5: University of Reading, Reading, RG6 6BB, U.K.

6: Met Office Hadley Centre, Joint Centre for Hydrometeorological Research, Wallingford, OX10 8BB, U.K.

* Corresponding Author

Keywords: Climate stabilisation, global warming, temperature thresholds, carbon cycle, methane cycle, permafrost thaw

Methane emissions from natural wetlands and carbon release from permafrost thaw have a positive feedback on climate, yet are not represented in most state-of-the-art climate models. Furthermore, a fraction of the thawed permafrost carbon is released as methane, enhancing the combined feedback strength. We present simulations with an intermediate complexity climate model which follow prescribed global warming pathways to stabilisation at 1.5°C or 2.0°C above pre-industrial levels by the year 2100, and that incorporates a state-of-the-art global land surface model with updated descriptions of wetland and permafrost carbon release. We demonstrate that the climate feedbacks from those two processes are substantial. Specifically, permissible anthropogenic fossil fuel CO_2 emission budgets are reduced by 17-23% (47-56 GtC) for stabilisation at 1.5°C, and 9-13% (52-57 GtC) for 2.0°C stabilisation. In our simulations these feedback processes respond faster at temperatures below 1.5°C, and the differences between the 1.5°C and 2°C targets are disproportionately small. This key finding is due to our interest in

transient emission pathways to the year 2100 and does not consider the longer term implications of these feedback processes. We conclude that natural feedback processes from wetlands and permafrost must be considered in assessments of transient emission pathways to limit global warming.

Background

The 2009 meeting of the United Nations' Framework Convention on Climate Change (UNFCCC) in Copenhagen formalised the aspiration to stabilise global warming at no more than 2°C above pre-industrial levels[1]. The subsequent UNFCCC Paris Agreement in 2015 raised the additional possibility of aiming for an even lower upper warming threshold of 1.5°C[2]. These targets will require large reductions in anthropogenic greenhouse gas (GHG) emissions, with sustained decreases of ~3% per annum[3,4] and development of technologies to remove carbon dioxide (CO_2) from the atmosphere. This is because the equilibrium global warming for current GHG concentrations may already be near 1.5°C[5]. Given the anticipated difficulty in keeping below the 1.5°C threshold, two key questions are being asked. First, what are the implications in terms of allowable anthropogenic emissions to keep warming below 1.5°C rather than 2.0°C? Second, what is gained climatically or environmentally by keeping below 1.5°C, i.e. are unwelcome climate impacts potentially avoided?

The climate change observed during recent decades has been strongly linked to human influences on atmospheric GHG composition, leading the 5th IPCC assessment to state: "it is extremely likely that human influence has been the dominant cause of the observed warming since the mid-20th century"[6]. However atmospheric GHG levels are affected both directly (via anthropogenic GHG emissions) and indirectly by human activity. Indirect effects include climate change-induced adjustments to the land-atmosphere and/or ocean-atmosphere GHG exchange fluxes. This was first modelled for the global carbon cycle by [7] who predicted a

significant flux of carbon to the atmosphere via increased plant and soil respiration under warming for a business-as-usual scenario. Similar analyses have been undertaken separately for additional methane (CH_4) release from wetlands[8,9] and additional carbon released from the long-term permafrost store[10-12]. The increase in global warming may be under-estimated for a prescribed anthropogenic emissions trajectory if these processes are not considered. In reference to policy objectives, the anthropogenic fossil fuel emission budgets (AFFEBs) to limit global warming to 1.5°C or 2.0°C may be significantly reduced from current assessments[6,13,14].

This research focusses on two key feedback processes which were not included in most models in the fifth phase of the Coupled Model Intercomparison Project (CMIP5)[15] and will only be included in a small fraction of models participating the sixth phase (CMIP6). These are the effects of carbon release from the long-term permafrost store as CO_2 and the increased CH_4 emissions from natural wetlands, and the coupling between the two effects where carbon from thawed permafrost is also released as CH_4[16,17]. These are particularly pertinent issues given that CH_4 has a larger Global Warming Potential (GWP) by equivalent weight than CO_2, and the recent resurgent growth in atmospheric CH_4[18].

In contrast to CMIP5 simulations, which modelled climatic and environmental responses to prescribed pathways in atmospheric concentrations, the objective here is to estimate the anthropogenic response to meet a specified global warming target. We develop an inverted form of climate model to follow prescribed temperature trajectories[19] and calculate the corresponding AFFEBs[13], including the two aforementioned feedback effects. The modelling framework is based on the coupled Joint UK Land Environment Simulator (JULES[20,21]) and Integrated Model Of Global Effects of climatic aNomalies (IMOGEN[22,23]) system (Methods). The approach taken is generic and may be employed in further research to answer a number of environmental policy related questions in terms of meeting specified warming thresholds.

Model Setup

We use JULES version 4.8 release, with the addition of a 14 layered soil column for both hydro-thermal[24] and carbon[25] dynamics (Methods). The JULES configuration includes representations of land-use and land-use change (LULUC) and ozone damage on plant stomata to address policy-relevant warming scenarios outside the scope of this paper. Full JULES details are given in Methods.

The major advancement in the IMOGEN configuration used for this study is the prescription of evolving global temperature trajectories. Following this inverted form (Figure SI.1b; Methods), changes in radiative forcing, ΔQ, are calculated as a function of the time-history of global warming which are then ascribed to compatible atmospheric compositions of GHGs. The anthropogenic contribution to atmospheric CO_2 is calculated whilst taking in to account changes to the land and ocean carbon stores, together with prescription or calculation of non-CO_2 greenhouse gases. Additional IMOGEN enhancements for this analysis include the calculation of atmospheric CH_4 concentration and effective radiative forcing, capturing the climate impacts on CH_4 release from natural wetlands (Methods).

Critical to our analysis is understanding emission pathways available to stabilise at either 1.5°C or 2.0°C of warming since pre-industrial times. As this will be strongly influenced by anthropogenic perturbation of the climate system to present day, we constrain the historical global temperature (ΔT_G) to the HadCRUT4 observational record[26] and atmospheric composition to the Representative Concentration Pathway (RCP) record[27] for the period 1850-2015. Future projections of the non-CO_2 atmospheric composition is taken from the IMAGE-3.0 implementation of Shared-Socioeconomic-Pathway (SSP) version 2 under RCP2.6 (SSP2_RCP-2.6_IMAGE)[28] (Methods).

We select three possible global warming pathways to stabilisation at the 1.5°C or 2.0°C targets by 2100 (Figure 1a and Figure SI.2), which are described using the formulation in [19] (Methods). Two of the considered trajectories follow the more traditional scenario of reaching asymptotes at 1.5°C and 2.0°C from below. The third asymptotes to 1.5°C after an overshoot to 1.75°C, representing far greater attempts of decarbonisation of the atmosphere towards the end of the 21st century. The overshoot trajectory allows investigation into hysteresis effects which may have path-dependent impact on temperature stabilisation, e.g. carbon release due to permafrost thaw.

Discussion

The atmospheric CO_2 concentrations and derived anthropogenic emission pathways from our control runs (i.e. with no natural wetland CH_4 nor permafrost carbon feedbacks) are displayed in Figure 1. Using this "standard" configuration of JULES, we estimate the interquartile range of the AFFEBs for 2015-2100 as 464-568 GtC to meet the 2°C target, and 227-283 GtC or 227-288 GtC to meet the 1.5°C target with or without the overshoot, respectively (Table 1). The AFFEBs are broadly linear in ΔT_G across the three scenarios, i.e. 378-480 GtC $°C^{-1}$ and 421-516 GtC $°C^{-1}$ for the 1.5°C and 2°C scenarios, respectively. These results agree with previous estimates of AFFEBs using different methods[13].

The 2°C scenario allows close to "business as usual" emissions for the coming decade followed by extensive emission reductions of 3.5-4.1% per year between 2030 and 2100. However, if society were to act more immediately, the AFFEB could be met with year-on-year reductions of 2.2-2.7% from 2020. The 1.5°C scenario with no overshoot indicates a near immediate peak in annual emissions followed by 3.5-4.3% year-on-year reductions from 2020. Despite the similarity of the AFFEB for the two 1.5°C scenarios, the overshoot scenario places larger pressure on future generations. This pathway implies that anthropogenic activities are a net

311-377 GtC source of CO_2 until the early-2050s, then must become a net sink, capturing 90.4-101 GtC. These estimates go further than previous attempts to quantify AFFEB[13,14] as they provide an AFFEB for each GCM, and the transient pathway, to meet the specified stabilised temperature.

The role of permafrost thaw in modulating the AFFEB is measured as the amount of carbon that was in the pre-industrial permafrost carbon store that is lost to the atmosphere. We define permafrost as soil layers within grid cells which JULES simulates as perennially frozen. We find our estimates of present day permafrost extent and loss rate to agree with the models assessed in [11] (Figure SI.3). Furthermore, a comparison with an observation dataset[29] demonstrates that our simulations reproduce a reasonable present day spatial coverage of permafrost (Figure SI.4). By 2100, the model ensemble estimates a median 138 Mha loss of permafrost area at 3m depth for the 1.5°C asymptote pathway and a median 239 Mha loss for the 2.0°C pathway (Figure 2a and Table SI.3). This degradation of permafrost results in an additional 40.0-46.3, 45.6-51.2 and 61.9-72.0 GtC of pre-industrial permafrost carbon which is no longer perennially frozen, relative to 2015, for the three temperature scenarios. Between 20% and 30% of this newly "thermally active" carbon has been released to the atmosphere, reducing AFFEBs by 11.6-13.8 GtC across the three scenarios (Figure 2d and Table 1– blue boxes in first column). The uncertainty range presented here is the interquartile range of the climate ensemble. We use a model configuration very close to the upper extreme of the process uncertainty presented in [10], hence our estimates represent an upper limit to the potential permafrost feedback. Applying the findings of [10] implies that a lower limit to the permafrost feedback would be roughly half of what is presented here (~5-7 GtC).

The differences in permafrost loss between scenarios appears less than previous estimates[30]. However, our estimates represent a transient snapshot at 2100 and not equilibrium conditions which will not be met for several centuries. The permafrost is not in equilibrium by 2100,

particularly the deeper soil layers which show a lagged response to changes in the surface air temperature (Figure 2a and 2b). This behaviour is similarly observed in the pre-industrial permafrost carbon stocks which are still being significantly depleted by year 2100 (Figure 2c and 2d). The loss-rate of pre-industrial permafrost carbon to the atmosphere is still increasing by 2100 as the total pool of soil carbon to respire continues to grow despite the stabilisation of surface air temperature. This highlights the time-scales involved in permafrost processes and indicates that permafrost thaw will continue to have large implications on anthropogenic emissions into the 22nd century even if temperatures have stabilised.

The response of the AFFEB to permafrost thaw is non-linear with respect to ΔT_G, i.e. 19.3-21.7 GtC °C^{-1} for the 1.5°C scenarios and 11.6-12.5 GtC °C^{-1} for the 2°C scenario. This implies that the permafrost feedback is faster at lower temperature changes, and keeping temperatures below 1.5°C, rather than 2°C, does not make large differences to AFFEBs to 2100. However, this behaviour is primarily a feature of our interest in the AFFEB to 2100 and the additional carbon released in the 2°C scenario will continue to have implications into the 22nd century.

The impact of the natural wetland CH_4 feedback on the AFFEBs is the sum of reduced carbon uptake of the atmosphere, ocean and land due to a higher atmospheric CH_4 concentration. The magnitude and distribution of the JULES natural wetland CH_4 emissions are driven primarily by wetland area and the soil temperature and carbon content (Methods). Our estimates of wetland extent and zonal distribution for the present day are within the range of state-of-the-art observation datasets[31,32] (Figure SI.4). To encapsulate a range of methanogenesis process uncertainty we include a temperature sensitivity ensemble by varying Q_{10} in Equation 1 (Methods). We use Q_{10} values calibrated to represent two wetland types identified in [33] ("poor-fen" and "rich-fen") and a third "low-Q_{10}" which gave increased importance to high latitude emissions (Methods). Our ensemble spread sufficiently describes the magnitude and distribution of present day CH_4 emissions from natural wetlands according to the models

assessed in a recent intercomparison study[34] (Figure SI.5). That said, there is still much uncertainty in natural wetland CH_4 emissions and future work will look to improve our model via more rigorous comparisons with observational datasets.

The global mean atmospheric CH_4 concentrations are increased by 3-9% and 6-15% (w.r.t. the control simulation) when the natural CH_4 feedback is included for the 1.5°C and 2°C target, respectively (Figure 3a for the "poor-fen" parameterisation and supplementary Figure SI.6 for the other parameterisations). The major driver of increased to CH_4 emissions is increased soil temperatures as changes in wetland extent and soil carbon content are not consistent globally (Figure SI.7). The increased atmospheric CH_4 concentrations imply reduced atmospheric CO_2 concentrations to ensure that simulations follow the prescribed temperature pathway (Figure 3b). The reduced atmospheric CO_2 concentrations result in reduced CO_2 fertilisation of vegetation and a slower oceanic drawdown of CO_2. Additionally, the increased ozone due to increased CH_4 (Methods) limits productivity further still. The AFFEBs are hence lowered by 33-51 GtC for the full temperature sensitivity ensemble (yellow cells in Table 1 and Figure 3d).

Similar to the permafrost feedback, the natural CH_4 feedback is non-linear with respect to ΔT_G, i.e. 55-71 GtC $°C^{-1}$ for the 1.5°C scenario and 34-46 GtC $°C^{-1}$ for the 2°C scenario. The effects of the natural CH_4 feedbacks are 13-21% larger for the 2°C scenario than the 1.5°C scenarios despite a temperature increase that is 83% larger, from present day. Furthermore, we found that this non-linear behaviour was maintained for the three temperature sensitivities considered in our uncertainty analysis (Figure 3d). Therefore, in the context of the natural wetland feedback strength, we conclude that constraining warming to less than 1.5°C, rather than 2°C, has a disproportionately small impact on the AFFEB.

198 The natural CH_4 feedback strength is slightly reduced for the 1.5°C with overshoot in
199 comparison to the 1.5°C asymptote pathway (Figure 3a). The two scenarios have similar
200 atmospheric CH_4 concentrations by 2100 (median difference < 5ppb) hence the atmospheric
201 CO_2 sinks in year 2100 are similar. However, the overshooting pathway has higher atmospheric
202 CO_2 concentrations during the 21st Century, hence the ocean and land sinks are not reduced by
203 as much. This implies that an overshooting pathway may be more robust to the natural CH_4
204 feedback as the land and ocean sinks are more effective. Given that the magnitude of this
205 difference is small, 1-2 GtC, it is difficult to generalise this behaviour.

206 Our simulations show little interaction (where thawed permafrost is released as CH_4) between
207 the feedback processes, i.e. the difference between the sum of the AFFEB differences and
208 AFFEB difference from the simulation including both feedback processes < 2 GtC. The amount
209 of CH_4 released from the thawed permafrost carbon is 0.2-0.6 $TgCH_4$ per year, where the upper
210 limit corresponds to the "low-Q_{10}" parameterisation (Figure SI.8a) which gave a greater
211 emphasis to CH_4 emissions from cooler regions (methods). This is ~0.16-0.56 % of global CH_4
212 emissions in 2015, decreasing to ~0.12-0.46% in 2100 (Figure SI.8b). Similarly, the fraction
213 of permafrost carbon released as CH_4 is 0.15-0.59% (Figure SI.8c). The additional atmospheric
214 CH_4 translates to changes of global atmospheric CO_2 of the order 0.1 ppmv, which has little
215 impact on the absolute atmospheric carbon sink nor the uptake of carbon by the land and ocean.
216 Hence, in the context of our estimates of AFFEBs to meet the UNFCC targets (200-500 GtC),
217 the interplay of these two feedback schemes is largely negligible. However, our modelling
218 framework does not account for thermokarst lakes created via ground subsidence following
219 permafrost thaw. To provide an estimate of uncertainty regarding this omission we emulate the
220 behaviour offline by linearly increasing wetland extent in permafrost regions through the 21st
221 Century, from a factor of 1 in year 2000 to a factor of 2 in year 2100 (Figure SI.10). The
222 increased CH_4 emissions reduces the AFFEB by a further 0.8-2.5 GtC. However, we see this

as an over-estimate as the emulation does not consider the reduced aerobic respiration due to increased saturated soil which has been shown to outweigh the increased CH_4 emissions[16].

Conclusions

The combined effect of these feedback processes has large implications on AFFEBs, 16.7-23.2% (46.6-55.7 GtC) and 9.5-13% (51.4-64.6 GtC) reductions for the 1.5°C and 2°C scenarios from the control runs, respectively (Table 1 – green cells). In terms of mitigation pathways this corresponds to 4.6-5.4% year-on-year reductions in anthropogenic emissions beginning in 2020 to meet the 1.5°C emission budget. To meet the 2°C warming target, the allowable emissions would require year-on-year reductions of 3.9-4.5% beginning in 2030, or 2.4-3.0% starting in 2020. This represents a 1-1.5% increase in reduction rates for the 1.5°C and only a 0.3-0.6% increase in reduction rates for the 2°C. The 1.5°C overshoot pathway indicates that total allowable anthropogenic emissions would need to be no more than 292-351 GtC prior to the mid-2050s followed by a removal of 101-118 GtC.

We find that to fulfil a 1.5°C warming threshold with no overshoot, increased CH_4 emissions from natural wetlands reduce the AFFEB between now and year 2100 by 12-17%. Carbon released from the long-term permafrost store reduces the AFFEB by an additional 4.1-5.3%, and the interplay between the two processes a further 0.5-1 %. This leaves AFFEBs of 175-235 GtC to 2100, a total reduction of 17-23%. Allowing for an overshoot to 1.75°C, but still leading ultimately to 1.5°C warming, makes little difference to the AFFEB, 172-240 GtC to 2100. However, such an eventuality would require significant developments of carbon capture technologies in the second half of the 21st century during which the net anthropogenic contribution to the carbon cycle would have to be a 101-118 GtC sink. The reduction in AFFEB for stabilisation at 2.0°C is, in absolute terms, similar to the reductions required to meet the 1.5°C target, 51.4-64.6 GtC. However, this is a much lower fraction of the AFFEB, 9.5-13.0%.

Our overall findings are that the natural climate feedbacks considered here are non-linear with respect to the AFFEB to meet a given temperature target by year 2100. Therefore, the role of the natural CH_4 and permafrost thaw feedback processes become increasingly more important when considering the lower stabilisation temperature target of 1.5°C.

References

1 UNFCCC. Copenhagen Accord FCCC/CP/2015/L.9/Rev. 1. (2009).
2 UNFCCC. Adoption of the Paris Agreement FCCC/CP/2015/L.9/Rev. 1. (2015).
3 Huntingford, C. *et al.* The link between a global 2 °C warming threshold and emissions in years 2020, 2050 and beyond. *Environmental Research Letters* **7**, 014039 (2012).
4 Rogelj, J., McCollum, D. L., Reisinger, A., Meinshausen, M. & Riahi, K. Probabilistic cost estimates for climate change mitigation. *Nature* **493**, 79-83 (2013).
5 Huntingford, C. & Mercado, L. M. High chance that current atmospheric greenhouse concentrations commit to warmings greater than 1.5 °C over land. **6**, 30294 (2016).
6 IPCC. in *Climate Change 2013: The Physical Science Basis. Contribution of Working Group I to the Fifth Assessment Report of the Intergovernmental Panel on Climate Change* (eds T.F. Stocker *et al.*) (Cambridge University Press, 2013).
7 Cox, P. M., Betts, R. A., Jones, C. D., Spall, S. A. & Totterdell, I. J. Acceleration of global warming due to carbon-cycle feedbacks in a coupled climate model. *Nature* **408**, 184-187, doi:10.1038/35041539 (2000).
8 Gedney, N., Cox, P. M. & Huntingford, C. Climate feedback from wetland methane emissions. *Geophysical Research Letters* **31**, doi:10.1029/2004gl020919 (2004).
9 Shindell, D. T., Walter, B. P. & Faluvegi, G. Impacts of climate change on methane emissions from wetlands. *Geophysical Research Letters* **31**, L21202, doi:10.1029/2004GL021009 (2004).
10 Burke, E. J. *et al.* Quantifying uncertainties of permafrost carbon–climate feedbacks. *Biogeosciences* **14**, 3051 (2017).
11 McGuire, A. D. *et al.* Variability in the sensitivity among model simulations of permafrost and carbon dynamics in the permafrost region between 1960 and 2009. *Global Biogeochemical Cycles* **30**, 1015-1037, doi:10.1002/2016GB005405 (2016).
12 Burke, E. J., Chadburn, S. E., Huntingford, C. & Jones, C. D. CO2 loss by permafrost thawing implies additional emissions reductions to limit warming to 1.5 or 2 °C. *Environmental Research Letters* **13**, 024024 (2018).
13 Millar, R. J. *et al.* Emission budgets and pathways consistent with limiting warming to 1.5°C. *Nature Geoscience*, 741-748, doi:10.1038/ngeo3031 (2017).
14 Tokarska, K. B. & Gillett, N. P. Cumulative carbon emissions budgets consistent with 1.5 °C global warming. *Nature Climate Change* **8**, 296-299, doi:10.1038/s41558-018-0118-9 (2018).
15 Taylor, K. E., Stouffer, R. J. & Meehl, G. A. An Overview of CMIP5 and the Experiment Design. *Bulletin of the American Meteorological Society* **93**, 485-498, doi:10.1175/bams-d-11-00094.1 (2012).
16 Schädel, C. *et al.* Potential carbon emissions dominated by carbon dioxide from thawed permafrost soils. *Nature Climate Change* **6**, 950, doi:10.1038/nclimate3054 (2016).
17 Schuur, E. A. G. *et al.* Climate change and the permafrost carbon feedback. *Nature* **520**, 171-179, doi:10.1038/nature14338 (2015).

18 Crill, P. M. & Thornton, B. F. Whither methane in the IPCC process? *Nature Climate Change* **7**, 678, doi:10.1038/nclimate3403 (2017).

19 Huntingford, C. *et al.* Flexible parameter-sparse global temperature time profiles that stabilise at 1.5 and 2.0 °C. *Earth Syst. Dynam.* **8**, 617-626, doi:10.5194/esd-8-617-2017 (2017).

20 Best, M. *et al.* The Joint UK Land Environment Simulator (JULES), model description–Part 1: energy and water fluxes. *Geoscientific Model Development* **4**, 677-699 (2011).

21 Clark, D. *et al.* The Joint UK Land Environment Simulator (JULES), model description–Part 2: carbon fluxes and vegetation dynamics. *Geoscientific Model Development* **4**, 701-722 (2011).

22 Huntingford, C. & Cox, P. M. An analogue model to derive additional climate change scenarios from existing GCM simulations. *Climate Dynamics* **16**, 575-586, doi:10.1007/s003820000067 (2000).

23 Huntingford, C. *et al.* IMOGEN: an intermediate complexity model to evaluate terrestrial impacts of a changing climate. *Geoscientific Model Development* **3**, 679-687, doi:10.5194/gmd-3-679-2010 (2010).

24 Chadburn, S. *et al.* An improved representation of physical permafrost dynamics in the JULES land-surface model. *Geoscientific Model Development* **8**, 1493-1508 (2015).

25 Burke, E. J., Chadburn, S. E. & Ekici, A. A vertical representation of soil carbon in the JULES land surface scheme (vn4. 3_permafrost) with a focus on permafrost regions. *Geoscientific Model Development* **10**, 959 (2017).

26 Morice, C. P., Kennedy, J. J., Rayner, N. A. & Jones, P. D. Quantifying uncertainties in global and regional temperature change using an ensemble of observational estimates: The HadCRUT4 data set. *Journal of Geophysical Research: Atmospheres* **117**, D08101, doi:10.1029/2011JD017187 (2012).

27 Meinshausen, M. *et al.* The RCP greenhouse gas concentrations and their extensions from 1765 to 2300. *Climatic Change* **109**, 213, doi:10.1007/s10584-011-0156-z (2011).

28 van Vuuren, D. P. *et al.* Energy, land-use and greenhouse gas emissions trajectories under a green growth paradigm. *Global Environmental Change* **42**, 237-250 (2017).

29 Brown, J., Ferrians Jr, O., Heginbottom, J. & Melnikov, E. (National Snow and Ice Data Center, 1998).

30 Chadburn, S. E. *et al.* An observation-based constraint on permafrost loss as a function of global warming. **7**, 340, doi:10.1038/nclimate3262 (2017).

31 Zhang, B. *et al.* Methane emissions from global wetlands: An assessment of the uncertainty associated with various wetland extent data sets. *Atmospheric Environment* **165**, 310-321, doi:https://doi.org/10.1016/j.atmosenv.2017.07.001 (2017).

32 Poulter, B. *et al.* Global wetland contribution to 2000–2012 atmospheric methane growth rate dynamics. *Environmental Research Letters* **12**, 094013 (2017).

33 Turetsky, M. R. *et al.* A synthesis of methane emissions from 71 northern, temperate, and subtropical wetlands. *Global Change Biology* **20**, 2183-2197, doi:10.1111/gcb.12580 (2014).

34 Saunois, M. *et al.* The global methane budget 2000–2012. *Earth Syst. Sci. Data* **8**, 697-751, doi:10.5194/essd-8-697-2016 (2016).

35 Jones, C. *et al.* The HadGEM2-ES implementation of CMIP5 centennial simulations. *Geoscientific Model Development* **4**, 543 (2011).

36 Zona, D. *et al.* Cold season emissions dominate the Arctic tundra methane budget. *Proceedings of the National Academy of Sciences* **113**, 40-45, doi:10.1073/pnas.1516017113 (2016).

37 McNorton, J. *et al.* Role of regional wetland emissions in atmospheric methane variability. *Geophysical Research Letters* **43**, 11,433-411,444, doi:10.1002/2016GL070649 (2016).

38 Clark, D. *et al.* The Joint UK Land Environment Simulator (JULES), model description - Part 2: Carbon fluxes and vegetation dynamics. *Geoscientific Model Development* **4**, 701-722, doi:10.5194/gmd-4-701-2011 (2011).
39 Gedney, N. & Cox, P. M. The sensitivity of global climate model simulations to the representation of soil moisture heterogeneity. *Journal of Hydrometeorology* **4**, 1265-1275 (2003).
40 Marthews, T., Dadson, S., Lehner, B., Abele, S. & Gedney, N. High-resolution global topographic index values for use in large-scale hydrological modelling. *Hydrology and Earth System Sciences* **19**, 91-104 (2015).
41 Klein Goldewijk, K., Beusen, A., Van Drecht, G. & De Vos, M. The HYDE 3.1 spatially explicit database of human-induced global land-use change over the past 12,000 years. *Global Ecology and Biogeography* **20**, 73-86 (2011).
42 Sitch, S., Cox, P. M., Collins, W. J. & Huntingford, C. Indirect radiative forcing of climate change through ozone effects on the land-carbon sink. *Nature* **448**, 791-794 (2007).
43 Stohl, A. *et al.* Evaluating the climate and air quality impacts of short-lived pollutants. *Atmos. Chem. Phys.* **15**, 10529-10566, doi:10.5194/acp-15-10529-2015 (2015).
44 Etminan, M., Myhre, G., Highwood, E. J. & Shine, K. P. Radiative forcing of carbon dioxide, methane, and nitrous oxide: A significant revision of the methane radiative forcing. *Geophysical Research Letters* **43**, 12,614-612,623, doi:10.1002/2016GL071930 (2016).
45 IPCC. *Climate change 2001: the scientific basis*. (The Press Syndicate of the University of Cambridge, 2001).

Corresponding Author

All correspondence and requests for materials should be made to Edward Comyn-Platt (edwcom@ceh.ac.uk).

Acknowledgements

The work was undertaken as part of the UK Natural Environment Research Council's programme "Understanding the Pathways to and Impacts of a 1.5°C Rise in Global Temperature" through grants NE/P015050/1 CLIFFTOP (E.C-P, G.H., S.C.), NE/P014909/1, MOC1.5 (W.C., C.W., C.H., P.C., S.S.) and NE/P014941/1 CLUES (P.C., T.P.). We also acknowledge the support for: (a) E.B. and N.G., the Joint UK BEIS/Defra Met Office Hadley Centre Climate Programme (GA01101); (b) E.B., CRESCENDO (EU project 641816); (c) A.H., EPSRC Fellowship "Negative Emissions and the Food-Energy-Water Nexus" (EP/N030141/1); and (d) C.H., CEH National Capability Funding. We also acknowledge the

wetland extent data products provided by Dr. B. Zhang, of Auburn University, USA and Dr. B. Poulter of the NASA Goddard Space Flight Center, USA.

Author Contributions

G.H., E.B., S.C. and E.C-P conceived and developed the project. E.C-P and C.H. led the development of the inverse IMOGEN model system. E.B. and S.C. contributed code and expertise on permafrost and soil carbon modelling. N.G., S.C. and E.C.P. contributed code and expertise on the JULES wetlands methane scheme. A.H. and T.P. contributed land use change, W.C. and C.W. ozone ancillary data and S.S. contributed expertise on the ozone damage effects, respectively. E.C-P., C.H., G.H., E.B., S.C., W.C., C.W., P.C., A.H. and T.P. contributed to the design of the IMOGEN model runs. All authors contributed to the interpretation of the results and to the writing of the paper.

Competing financial interests

The authors declare no competing financial interests.

Methods

(1) The JULES model[20,21].

(a) Model version and configuration

JULES is a process-based land surface model that simulates energy, water and carbon fluxes at the land-atmosphere boundary. JULES can be run as a standalone model using given meteorological driving variables or as the land surface component of climate modelling systems of varying degrees of complexity, e.g. Earth System Models[35] or IMOGEN[18]. We use the JULES version 4.8 release with the addition of a 14 layered soil column over 3m for both hydro-thermal[24] and carbon dynamics[25]. Burke et al.,[25] demonstrated that modelling the soil carbon fluxes as a multi-layered scheme improves estimates of soil carbon stocks and net ecosystem exchange. In addition to the vertically discretised respiration and litter input terms, the soil carbon balance also includes a diffusivity term which represents cryoturbation/bioturbation processes. The freeze-thaw processes of cryoturbation is particularly important in cold permafrost type soils[10].

The multi-layered methanogenesis scheme improves the representation of high latitude CH_4 emissions where previous studies underestimated production at cold permafrost sites during "shoulder seasons"[36]. The multi-layered scheme allows an insulated sub-surface layer of active methanogenesis to continue after the surface has frozen. These model developments not only improve the seasonality of the emissions, but more importantly for this study capture the release of carbon as CH_4 from deep soil layers, including thawed permafrost. The formulation of the multi-layered scheme gives the local land-atmosphere CH_4 flux, E_{CH4} (kg C m^{-2} s^{-1}), as:

$$E_{CH4} = k \cdot f_{wetl} \cdot \sum_{C_s\ pools}^{i} \kappa_i \cdot \sum_{z=0\mathrm{m}}^{z=3\mathrm{m}} e^{-\gamma z} C_{s_{i,z}} \cdot Q_{10}\left(T_{soil_z}\right)^{0.1\left(T_{soil_z} - T_0\right)} \qquad \textit{Equation 1}$$

Where z is the depth in soil column (in m), i is the soil carbon pool, f_{wetl} (-)is the fraction of wetland area in the gridcell, κ_i (s^{-1}) is the specific respiration rate of each pool (Table 8 of [21]), C_s (kg m^{-2}) is soil carbon, T_{soil} (K) is the soil temperature. γ (= 0.4 m^{-1}) is a constant that describes the reduced contribution of CH_4 emission at deeper soil layers due to inhibited transport and increased oxidation through overlaying soil layers. This is a simplification, however previous work which explicitly represented these processes showed little to no improvement when compared with in-situ observations[37]. The four soil carbon pools (i) in JULES are decomposable plant material, resistant plant material, microbial biomass, and humus. As JULES is a processed based model, the carbon emitted as CH_4 is therefore removed from the soil carbon stock. Furthermore, as described in [38], soil respiration is non-zero in fully saturated soils, hence in anaerobic conditions JULES produces CO2 in addition to CH4.

f_{wetl} is calculated using the JULES implementation of TOPMODEL[39] as the integral of a normalised gamma distribution of a prescribed topographic index dataset[40], $G(\tau)$, between a critical, τ_{crit} (ln(m)), and maximum, τ_{max} (ln(m)), topographic index, i.e.:

$$f_{wetl} = \int_{\tau_{crit}}^{\tau_{max}} G(\tau)d\tau, \qquad \textit{Equation 2}$$

τ_{crit} is dependent on the local water table as:

$$\tau_{crit} = ln\left(\frac{\Psi(0)}{\Psi(\overline{z_w})}\right) + \bar{\tau}, \qquad \textit{Equation 3}$$

where $\Psi(0)$ and $\Psi(\overline{z_w})$ ($m^2 s^{-1}$) are the transmissivities of entire soil column and the soil column below the mean water table depth, $\overline{z_w}$ (m). The τ_{max} limit excludes regions where the water table is sufficiently high enough for stream flow and hence assumed to be a negligible emitter of CH_4. It is calculated as:

$$\tau_{max} = \tau_{crit} + \tau_{range}, \qquad \textit{Equation 4}$$

where τ_{range} (= 2.0) is a global tuning parameter.

$\overline{z_w}$ is incrementally updated based on the balance of water flux processes on each JULES timestep. When $\overline{z_w}$ is in the deep store (a singular 15 m below the 14 modelled layers) it is updated as the balance between the infiltration water, I_{Deep}, and the baseflow, B_{Deep}, as:

$$\rho\theta_{sat}\frac{d(\overline{z_w})}{dt} = I_{Deep} - B_{Deep}, \qquad \textit{Equation 5}$$

where ρ is the density of water and θ_{sat} is the saturated volumetric water content. If the deep layer is fully saturated $\overline{z_w}$ is calculated diagnostically to be in the deepest unsaturated model soil layer. The water content of each layer, j, is updated on each time step as the balance of the vertical flux processes (infiltration, I_j, and Evapotranspiration, E_j), and, for layers below $\overline{z_w}$, a horizontal baseflow flux, B_j, i.e.:

$$\Delta z_j \rho\frac{d(\theta_j)}{dt} = I_j - E_j - B_j, \qquad \textit{Equation 6}$$

where Δz_j is the thickness and θ_j is the volumetric water content of j^{th} soil layer. For full details of the process based JULES hydrology please refer to [20] and [39].

In addition, the JULES configuration includes prescribed land-use and land-use change (LULUC), where land used for agriculture can only grow C3 and C4 grasses to represent crops and pasture. The land-use mask consists of an annual fraction of agricultural land in each grid cell. Historical LULUC is based on the HYDE 3.1 dataset[41], and future LULUC is based on the SSP2_RCP-2.6_IMAGE[28]. When natural vegetation is converted to managed agricultural land, the removed vegetation carbon is placed into woody product pools that decay at various rates back into the atmosphere[35]. The carbon flux from LULUC is therefore not lost from the system.

We use a JULES configuration including ozone deposition damage to plant stomata, which then affects land-atmosphere CO_2 exchange[42]. JULES requires surface atmospheric ozone concentrations, O_3 (ppb), for the duration of the simulation period (1850-2100). Here, we use

two sets of monthly O_3 concentration fields calculated using the HADGEM3-A GA4.0 model for low (1285 ppbv) and high (2062 ppbv) global mean atmospheric CH_4 concentrations[43]. We regrid these fields (1.875°x1.25° horizontal grid) to the spatial grid of IMOGEN-JULES (3.75°x2.5° horizontal grid). We then linearly interpolate between the respective months in the regridded O_3 fields using the global annual atmospheric CH_4 concentration. The CH_4 concentration is taken from the prescribed SSP2_RCP-2.6_IMAGE plus the natural CH_4 modulation when the interactive scheme is in use.

(b) Wetland CH_4 emission scheme calibration

We calibrate the temperature sensitivity of the multi-layered methanogenesis scheme (k and $Q_{10}(T_{soil}) = Q_{10}$^[$T_0$/$T_{soil}$] in Equation 1) for each CMIP5 model in the IMOGEN ensemble to ensure the wetland CH_4 production rates match present day observations[33,34]. [33] fit observed surface CH_4 fluxes, E_{CH4}, against temperature to Equation 7 using data from 71 sites:

$$E_{CH4\_Turetsky} = A_{Turetsky} \times Q_{10\_Turetsky}^{0.1T_{soil-10cm}}, \qquad \textit{Equation 7}$$

where $T_{soil\text{-}10cm}$ is the temperature of the top 10 cm of soil.

To capture temperature sensitivity uncertainty we calibrate Q_{10} in Equation 1 against Equation 7 for 2 of the wetland types identified in [33] ("Poor Fen" and "Rich Fen") using the daily output from the JULES-simulations at the year 2000 for each GCM. We select Q_{10} values which maximise the Pearson's correlation coefficient. k is then calculated such that the global total for the year 2000 is 180 $TgCH_4$ to match our assumptions of the atmospheric growth rate of CH_4 in the IMOGEN CH_4 feedback calculations (see IMOGEN description below). We selected the "Poor Fen" and "Rich Fen" parameterisations for our ensemble as these gave the best representation of the global distribution of CH_4 emissions when compared with the output from [34] (Figure SI.9). A "Bog" parameterisation was ruled out as this tended towards unrealistically high tropical emissions, a "Swamp" parameterisation was ruled out due to the

high levels of uncertainty reported in [33]. The optimised parameter values are given in Table SI.2 of the Supplementary Information. In addition to the two calibrated parameterisations we include a "lowQ_{10}" (Q_{10}=2.0, k=1.625x10^{-9}) parameterisation which gave a larger fraction of global emissions to lower temperature regions (Figure SI.9).

(2) IMOGEN, EBM Inversion and the CMIP5 models selected for its calibration.

(a) IMOGEN[23] is a climate-carbon cycle model of intermediate complexity that uses "pattern-scaling" of the seven meteorological variables required to drive JULES. Huntingford, et al. [23] assume that changes in local temperature, precipitation, humidity, wind-speed, surface shortwave and longwave radiation and pressure are linear in global warming. Patterns are multiplied by the amount of global warming over land, ΔT_L, to give local monthly predictions of climate change. When using IMOGEN in forward mode, ΔT_L is calculated with an Energy Balance Model (EBM) as a function of the overall changes in radiative forcing, ΔQ (W m^{-2}). ΔQ is the sum of the atmospheric greenhouse gas contributions[44], updated on a yearly timestep.

Our simulations include a CH_4 feedback system that captures the climate impacts on CH4 emissions from natural wetland sources. The approach here follows that of [8] where prescribed CH_4 concentrations, which assume a non-varying natural wetland CH_4 component[28], are perturbed using the anomaly in modelled natural wetland CH_4 emission. To ensure consistency with the observed atmospheric CH_4 growth rate we calibrate our model to produce 180 $TgCH_4$ per year for the year 2000, as detailed in the model calibration description above. The increased/reduced atmospheric CH4 concentration will have corresponding longer/short atmospheric lifetime, λ, than the prescribed concentration pathway. We account for changes in λ following the formulation and parameterisation of [45], i.e. λ=8.4 yr^{-1} for an atmospheric CH_4 concentration of 1745ppb. The changes in radiative forcing were calculated using the formulation in [44]. There is large uncertainty in the natural wetland contribution to global CH_4

emissions, for this study we scale to 180 $TgCH_4$ per year, approximation based on a recent model intercomparison study[34] (Figure SI.6). Additionally, the effect of increased atmospheric CH_4 concentrations on tropospheric ozone levels is also accounted for, both in terms of radiative forcing and the impact on surface functioning through stomatal damage (see JULES description in Methods section 1a).

Previous IMOGEN studies[23,10] used 22 of the Earth System models (ESMs) involved in CMIP3 (phase 3 of the Coupled Model Intercomparison Project). Here, we update and extend IMOGEN to use Earth System models (ESMs) involved in CMIP5. We downloaded CMIP5 data from the mirror database held on the UK JASMIN computer during Autumn 2015. Table SI.1 lists every model for which historical monthly *surface temperature* fields were available.

The key criteria for inclusion of the output from a given CMIP5 GCM simulation is as follows (see Supplementary Information and Table SI.1):

1. Availability for the internal Energy Balance Model of surface temperature, top of the atmosphere (TOA) incoming shortwave radiation, outgoing TOA shortwave and longwave radiation;
2. Availability of meteorological parameters to drive JULES: surface temperature, precipitation, surface relative humidity, surface downward shortwave radiation, surface downward longwave radiation, surface wind speeds and surface pressure
3. Availability of two RCP scenarios for calibration and testing

(b) Energy Balance Model (EBM) Inversion. The EBM was inverted such that a change in radiative forcing, ΔQ, is calculated as a function of a change in the global temperature, ΔT_g (K), re-ordering of Equation (10) from Huntingford and Cox [22] gives:

$$\Delta Q(t) = f\left[\Delta T_o\left[\frac{(1-f)\lambda_l \nu}{f} + \lambda_o\right] - \kappa \left.\frac{\partial \Delta T_{o,s}}{\partial z}\right|_{z=0}\right], \qquad \textit{Equation 8}$$

Where $\Delta Q(t)$ is the change in radiative forcing (W m^{-2}) at time *t*, *f* is the fraction of Earth that is ocean, λ_l and λ_o are the climate sensitivities over land and ocean, respectively (W m^{-2} K^{-1}), ν is the land-sea contrast and κ is the ocean diffusivity (W m^{-1} K^{-1}). The values of the parameters f, λ_l, λ_o, ν and κ are unique to each GCM in the ensemble and are listed in the Supplementary Information, Table SI.2.

The change in the depth-dependent ocean temperature (ΔT_O) (K) must satisfy the diffusivity equation:

$$c_p \frac{\partial \Delta T_{o,s}}{\partial t} = \kappa \frac{\partial^2 \Delta T_{o,s}}{\partial z^2}, \qquad \textit{Equation 9}$$

where c_p is (J K^{-1} m^{-3}) is the specific heat capacity of salt water and z (m) is ocean depth (positive downwards). The change in the global mean surface ocean temperature (z=0) is then calculated from the global temperature, ΔT_G as [22]:

$$\Delta T_O = \frac{\Delta T_G}{[f + \nu - f\nu]}. \qquad \textit{Equation 10}$$

The global mean land temperature, ΔT_L, required for the "pattern scaling" was calculated as:

$$\Delta T_L = \nu \Delta T_O \qquad \textit{Equation 11}$$

(c) Etminan CO_2 Radiative Forcing Inversion.

Etminan et al.[44] present a formulation to calculate the change in radiative forcing, ΔQ_{CO_2}, from a given change in the global mean atmospheric CO_2 concentration. There is no exact solution for the inverse of this, i.e. to calculate the change in CO_2 for a given ΔQ_{CO_2}. We find the solution iteratively using Equation 3:

$$CO_{2_{i+1}} = CO_{2_{\mathrm{REF}}} \times e^{\left[\frac{\Delta Q_{CO_2}}{a_1(CO_{2_i} - CO_{2_{\mathrm{REF}}})^2 + b_1(CO_{2_i} - CO_{2_{\mathrm{REF}}}) + c_1\bar{N} + 5.36}\right]} \qquad \textit{Equation 12}$$

535 We assume convergence has occurred if the CO_2 concentration changes by less than 0.001
536 ppm. The initial CO_2 concentration for the iteration is taken to be the CO_2 concentration for
537 the previous year. We typically find that no more than 5 iterations are required for a change of
538 10 ppm from the starting concentration.

539 **(d) Q non-CO2 calculation.** Changes in radiative forcing, ΔQ (Wm^{-2}), calculated by the
540 inverted IMOGEN EBM must be ascribed to changes in the atmospheric composition of GHGs.
541 For this simplified description we consider two forcing contributions. The CO_2 forcing, ΔQ_{CO2}
542 (Wm^{-2}), and the forcing of all other agents, $\Delta Q_{\mathrm{nonCO2}}$ (Wm^{-2}). In the simplest case (not
543 considering interactive CH_4), a prescribed $\Delta Q_{\mathrm{nonCO2}}$, is removed from ΔQ to give ΔQ_{CO2} as:

$$\Delta Q_{CO2} = \Delta Q - \Delta Q_{non\,\mathrm{CO2}}. \qquad \textit{Equation 13}$$

544 The non-CO_2 composition is taken from the SSP2_RCP-2.6_IMAGE pathway[28]. The
545 SSP2_RCP-2.6_IMAGE pathway was chosen as it assumes very high GHG mitigation and the
546 global warming pathway is reasonably close to the 1.5°C or 2.0°C targets of interest (i.e. 1.8
547 °C by 2100). This prescribed non-CO_2 radiative forcing is subtracted from ΔQ to give the CO_2
548 radiative forcing ($\Delta Q_{CO2} = \Delta Q - \Delta Q_{non\,CO2}$). The CO_2 concentration is then derived using an
549 iterated inversion of the CO_2 radiative forcing equation in Etminan et al.[44] (Methods). For a
550 given $\Delta Q_{non\,CO2}$, we then estimate the CO_2 concentration iteratively, as described above, using
551 Equation 3.

552 Each of the 34 GCMs that IMOGEN emulates has a different set of EBM parameters - λ_l, λ_o, ν,
553 κ and f. Hence each GCM has a different ΔQ estimate for a given $\Delta T_G(t)$ pathway. When
554 IMOGEN is driven with a historical record of ΔT_G the range of ΔQ for the present day (2015)
555 is 1.13 W m^{-2} (Supplementary Information Figure SI.5a). For this work, we require the
556 historical period, 1850-2015, to match observations of both ΔT_G and atmospheric composition
557 for all GCMs. We, therefore, attribute the spread in ΔQ to uncertainty in $\Delta Q_{\mathrm{non\,CO2}}$, particularly

the atmospheric aerosol contribution which has an uncertainty range of -0.5 to -4 Wm^{-2} [6]. Given this, and to ensure continuous functions of ΔQ_{CO2} and $\Delta Q_{non\ CO2,}$ we calculated the contributions as:

$$\Delta Q_{\mathrm{CO2}}(t) = \begin{cases} \Delta Q_{\mathrm{CO2}}(\mathrm{t})_{SSP}, & t \leq 2015 \\ \Delta Q(t) - \Delta Q_{\mathrm{non}\ CO2}(t), & t > 2015 \end{cases}$$

$$\Delta Q_{\mathrm{non}\ CO2}(t) = \begin{cases} \Delta Q(t) - \Delta Q_{CO2}(t)_{SSP}, & t \leq 2015 \\ \Delta Q_{\mathrm{non\ CO2}}(t)_{SSP} + c(\mathrm{GCM}), & t > 2015 \end{cases}$$

Equation 14

where the subscript SSP indicates the value is sourced from SSP2_RCP-2.6_IMAGE. c (Wm^{-2}) is a GCM specific offset which ensured continuous ΔQ_{CO2} or $\Delta Q_{non\ CO2}$ and was calculated at the transitional year (2015) as:

$$c(GCM) = \Delta Q_{\mathrm{non}\ CO2}(2015) - \Delta Q_{\mathrm{non\ CO2}}(2015)_{SSP} \qquad \textit{Equation 15}$$

Figure SI.5 in the supplementary information shows the allocation of the ΔQ and the resultant atmospheric CO_2 concentration pathways for the 2°C stabilisation temperature. We include the GCM specific 2015 aerosol-offsets in Table SI.2 in the Supplementary Information.

(3) Temperature Profile Formulation. [19] provides a framework to create temperature trajectories based on two parameters which model the efforts of humanity to limit emissions and, if necessary, capture atmospheric carbon, i.e.:

$$\Delta T(t) = \Delta T_0 + \gamma t + \left(1 - e^{-\mu(t)t}\right)[\gamma t - (\Delta T_{\mathrm{Lim}} - \Delta T_0)] \qquad \textit{Equation 16}$$

where, $\Delta T(t)$ is the change in temperature from pre-industrial levels at year *t*, ΔT_0 is the temperature change at a given initial point (in this case $\Delta T_0 = 0.89$°C for 2015), ΔT_{Lim} is the final prescribed warming limit and:

$$\mu(t) = \mu_0 + \mu_1 t, \qquad \textit{Equation 17}$$

$$\gamma = \beta - \mu_0(\Delta T_{\mathrm{Lim}} - \Delta T_0).$$

Where β (= 0.00128) is the current rate of warming and the μ_0 and μ_1 are tuning parameters which describe anthropogenic attempts to stabilise global temperatures[19]. The selected parameterisation of the three trajectories are based on comparisons with CMIP5 simulations for the RCP2.6 scenario (grey lines in Figure SI.2). The parameter values used for the three profiles selected are shown below.

Profile	ΔT_{lim}	μ_0	μ_1
1.5°C	1.5	0.1	0.0
1.5°C (overshoot)	1.5	-0.01	0.00085
2°C	2.0	0.08	0.0

(4) Code and Data Availability

The data that support the findings of this study are available from the corresponding author upon request. The IMOGEN patterns and the model output required to produce the resulted presented herein will shortly be made publicly available for download on the EIDC.

JULES is an open-source model and the branch used in this work is available from the met-office science repository using the following URL (registration required):

https://code.metoffice.gov.uk/trac/jules/browser/main/branches/dev/edwardcomynplatt/vn4.8_1P5_DEGREES?rev=11764

The parameterisations used here are also permanently stored on the met-office science repository. Given the complexities in accessing the specific revision and machine configuration, these will be made available upon request to the corresponding author.

Figures

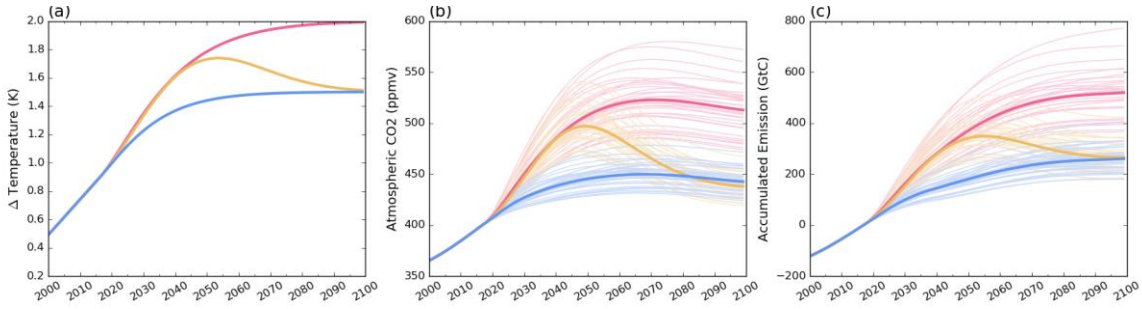

Figure 1 Time-series for the control model ensemble. Blue is the 1.5°C asymptote pathway, yellow is the 1.5°C overshoot pathway and red is the 2°C asymptote pathway. Faint lines are the individual GCMs, bold lines represent the ensemble median, and the colours are consistent across the panels. (a) Temperature pathways; (b) simulated atmospheric CO_2 concentrations; (c) derived allowable anthropogenic emissions.

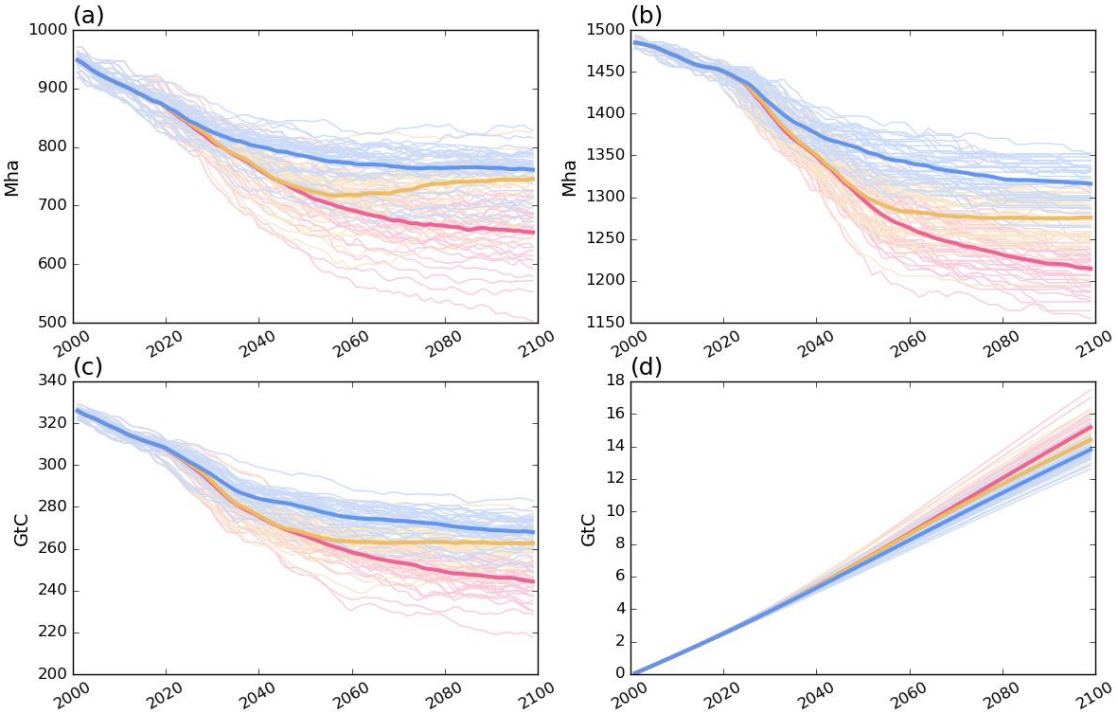

Figure 2 The response of the permafrost soil column to warming through the 21st century. (a) Areal extent of permafrost within the top 1m of soil column; (b) areal extent of permafrost within the top 3m of soil column; (c) the amount of pre-industrial permafrost carbon still perennially frozen; (d) the amount of pre-industrial carbon lost to the atmosphere. Blue is the 1.5°C asymptote pathway, yellow is the 1.5°C overshoot pathway and red is the 2°C asymptote pathway

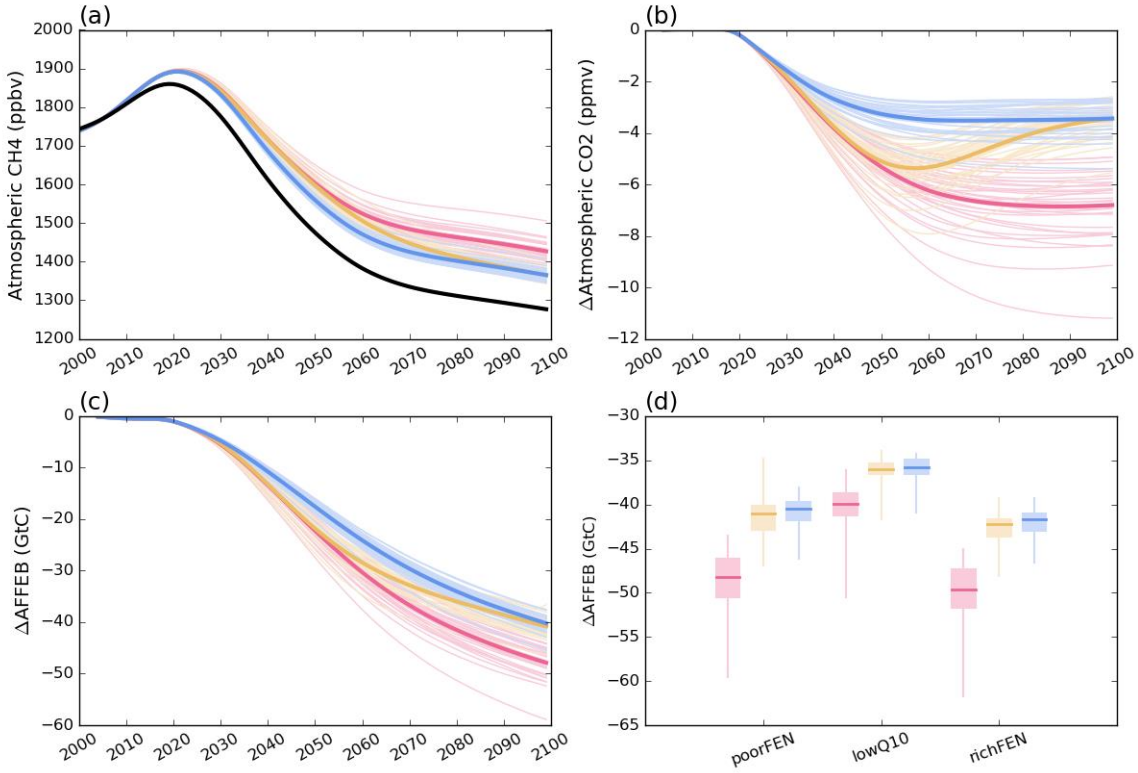

Figure 3 Summary results for the natural methane feedback experiment. (a) Time-series of atmospheric CH_4 when the interactive natural CH_4 is included ("poor fen" parameterisation) for the three temperature pathways. The black line is the control simulation atmospheric CH_4. (b) The reduction in atmospheric CO_2 (from control simulation) to follow the prescribed temperature pathway. (c) The reduction in anthropogenic fossil fuel emissions due to reduced atmosphere, land and ocean sinks. (d) The reduction in AFFEB for the temperature sensitivity uncertainty ensemble. Blue is the 1.5°C asymptote pathway, yellow is the 1.5°C overshoot pathway and red is the 2°C asymptote pathway.

598

599 **Tables**

Total Anthropogenic CO_2 emissions (GtC)				
		Standard	Methane Feedback	Difference
1.5°C	Standard	**265** (226-283)	**226** (187-249)	**39.6** (33.1-42.1)
	Permafrost Feedback	**254** (214-276)	**214** (175-235)	**40.1** (34.7-42.4)
	Difference	**11.9** (11.6-12.2)	**12.5** (11.9-14.0)	**52.1** (46.6-54.2) **19.4 %** (16.7-22.9 %)
1.5°C overshoot	Standard	**271** (227-288)	**232** (185-254)	**40.2** (33.6-42.8)
	Permafrost Feedback	**258** (214-276)	**218** (172-240)	**40.6** (36.3-43.1)
	Difference	**12.5** (12.1-13.0)	**13.0** (12.4-14.3)	**53.5** (47.4-55.7) **19.5 %** (16.6-23.2 %)
2°C	Standard	**527** (464-568)	**504** (417-528)	**47.4** (37.3-51.0)
	Permafrost Feedback	**514** (451-554)	**467** (404-514)	**47.8** (38.6-51.3)
	Difference	**13.3** (12.8-13.8)	**13.6** (13.0-15.0)	**61.1** (51.4 -64.6) **11.4 %** (9.5-13.0 %)

Table 1 Emission budgets from the factorial experiment and the changes due to the introduction of the feedback processes. White cells represent the absolute emission budget for the 2015-2100 period, blue cells represent the change due to inclusion of carbon released from the permafrost store, yellow cells represent the change due to inclusion of an interactive CH_4 scheme and green cells represent the change due to inclusion of both permafrost and interactive CH_4 feedbacks. Bold values give the climate ensemble median for the "poor fen" CH_4 parameterisation. Bracketed values represent the spread of the climate ensemble interquartile ranges for the 3 temperature sensitivity experiments (i.e. the full spread of the boxes in Figure 3b).

600